A Coal-Derived Carbon Fiber Scaffold with Superior Mechanical Robustness for Ultra-Stable Lithium Metal Anodes

Xian Lu [a], Qingtao Ma[a*], Xiaoquan Zhu[b*], Mengjiao Xu[a], Nannan Guo[a], Lili Ai[a], Changyu Leng[a], Luxiang Wang[a*]

[a]State Key Laboratory of Chemistry and Utilization of Carbon-Based Energy Resources, College of Chemistry, Xinjiang University, Urumqi 830017, Xinjiang, PR China

[b]College of Textiles and Clothing, Xinjiang University, Urumqi 830017, Xinjiang, PR China

*Corresponding authors

E-mail: qingtaoma@xju.edu.cn; zhuxiaoquan@xju.edu.cn; wangluxiangxju@163.com

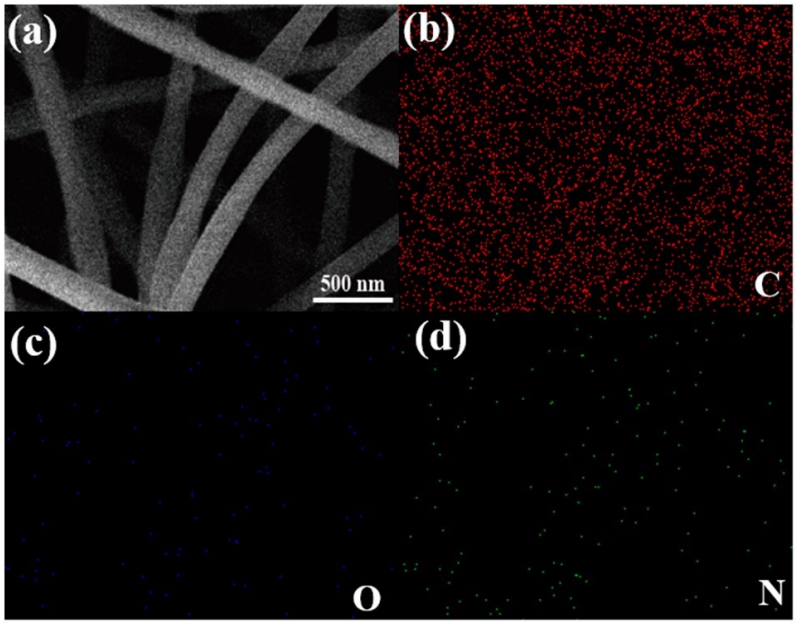

Fig. S1. (a) SEM plots and (b-d) corresponding elemental mappings of CBCNFs.

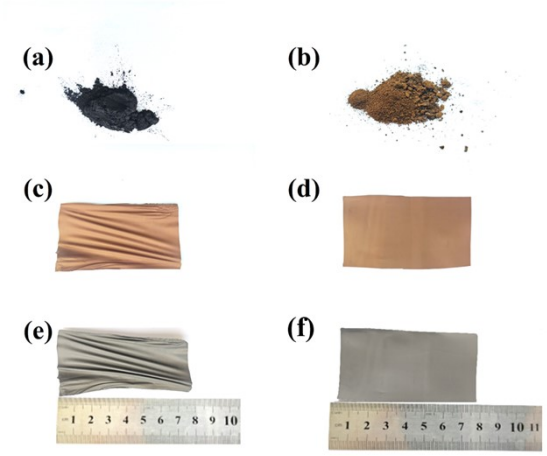

Fig. S2. Digital photograph of (a) raw coal, (b) oxidized coal, (c) CNFs and (d) CBCNFs after pre-oxidation and (e) CNFs and (f) CBCNFs after carbonation.

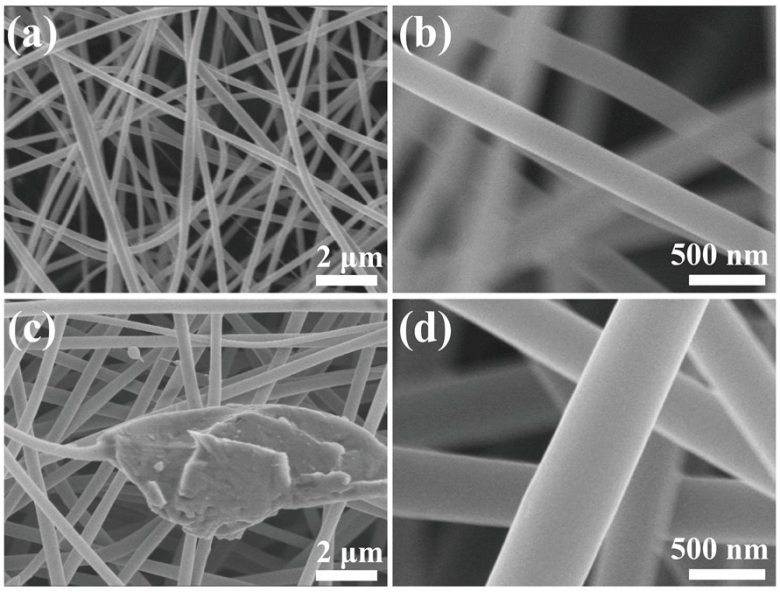

Fig. S3. Scanning electron microscope images of CBCNFs-1 (a-b) and CBCNFs-2 (c-d)

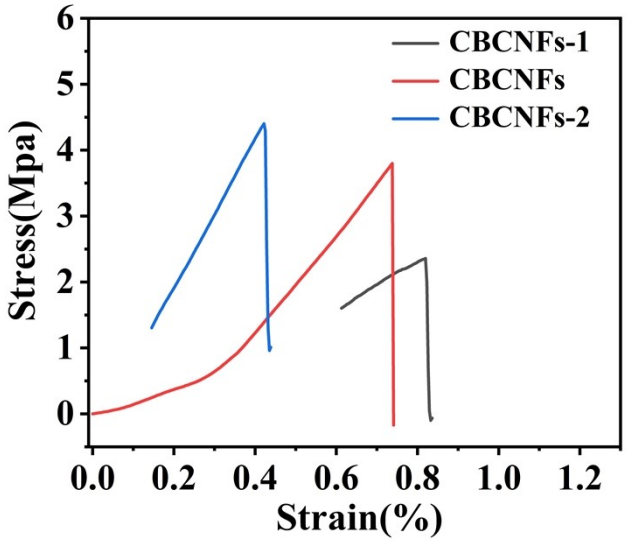

Fig. S4. Tensile strength of CBCNFs-1、CBCNFs and CBCNFs-2.

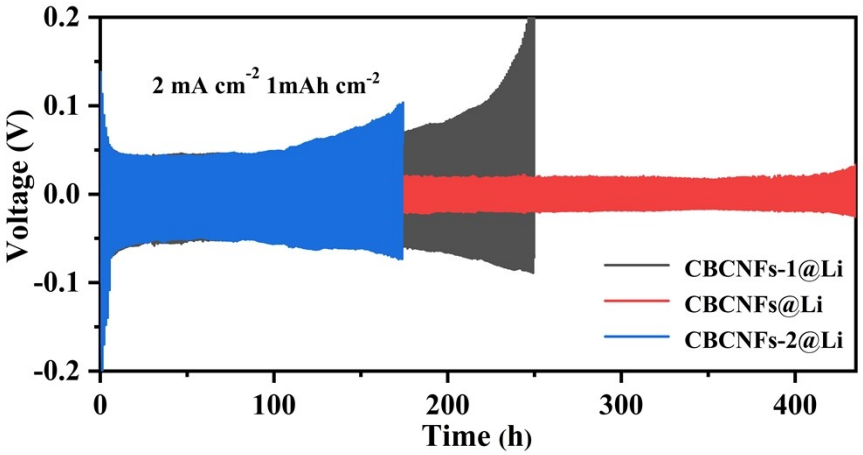

Fig. S5. The Voltage-time curves of CBCNFs-1@Li, CBCNFs@Li, and CBCNFs-2@Li symmetric batteries at a current density of 2 mA cm^{-2} and an area capacity of 1 mAh cm^{-2}.

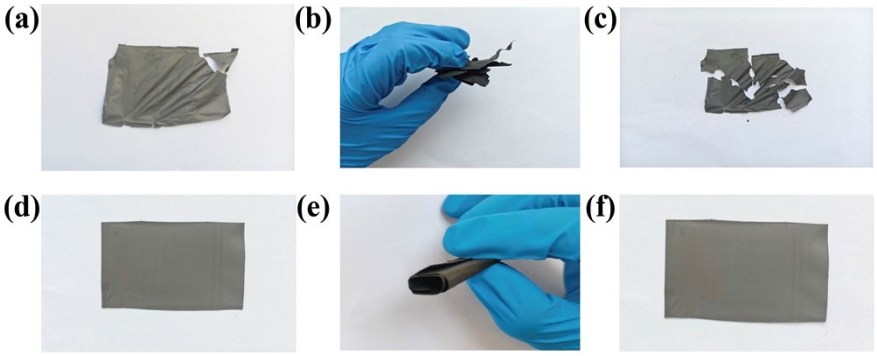

Fig. S6. Flexibility tests of (a-c) CNFs, (d-f) CBCNFs.

Table S1. Specific surface area and pore structure parameters of the samples.

Samples	$^{a}S_{BET}$ $m^2\ g^{-1}$	$^{b}V_{total}$ $cm^3\ g^{-1}$	$^{c}V_{micro}$ $cm^3\ g^{-1}$	V_{micro}/V_{total} %	$^{e}D_{ap}$ nm
CNFs	436.27	0.189	0.124	65.61	1.70
CBCNFs	551.25	0.187	0.154	82.35	1.36

Table S2. summary of elemental content analysis of XPS spectra of prepared samples.

Sample	C 1s (at%)	N 1s (at%)	O 1s (at%)
CNFs	85.13	10.33	4.54
CBCNFs	86.21	5.72	7.75

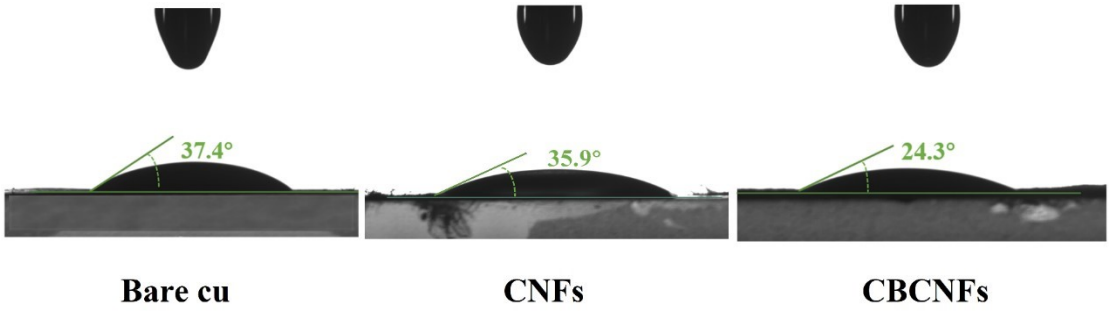

Fig. S7. Contact angle of ether-based electrolyte droplets on (a) bare copper, (b) CNFs, and (c) CBCNFs.

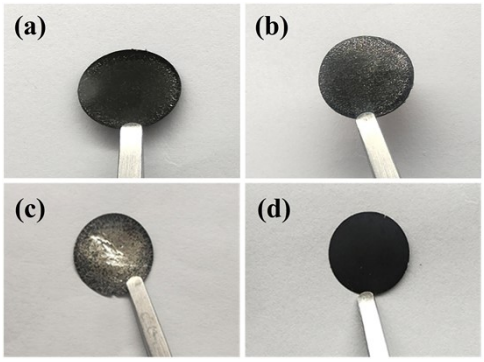

Fig. S8. Digital photograph of CBCNFs at different lithium plating capacities: (a) 5 mAh cm^{-2}, (b) 8 mAh cm^{-2}, (c) 10 mAh cm^{-2}, (d) after being charged to 1 V.

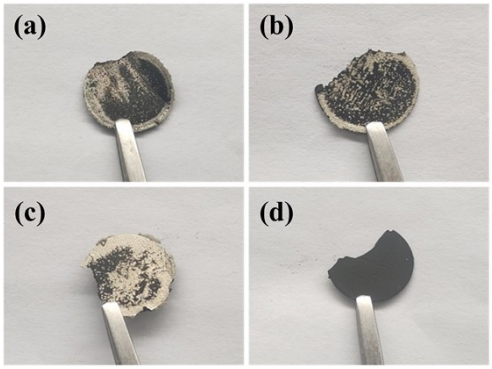

Fig. S9. Digital photograph of CNFs at different lithium plating capacities: (a) 5 mAh cm^{-2}, (b) 8 mAh cm^{-2}, (c) 10 mAh cm^{-2}, (d) after being charged to 1 V.

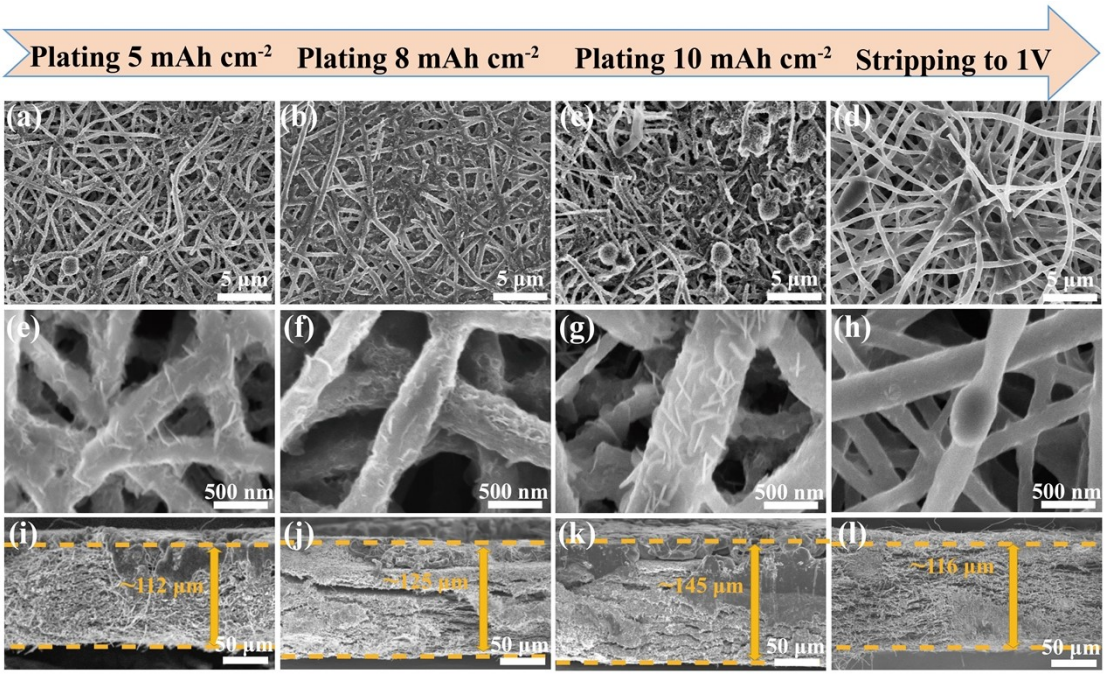

Fig. S10. The SEM images of CNFs after different lithium depositions are (a, e) 5 mAh cm^{-2}, (b, f) 8 mAh cm^{-2}, (c, g) 10 mAh cm^{-2} and (d, h) corresponding cross-sectional images after charging to 1 V (i-l).

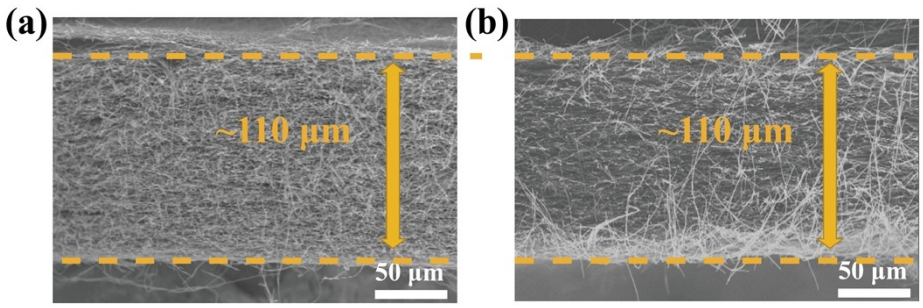

Fig. S11. Cross-sectional SEM images of (a) CBCNFs and (b) CNFs before electroplating.

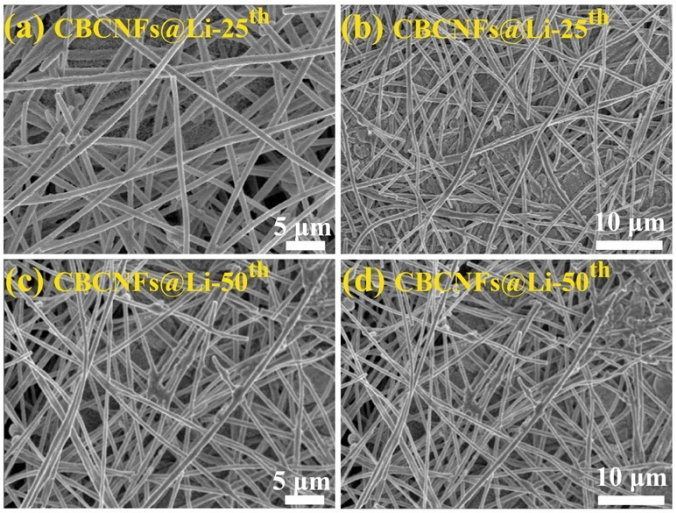

Fig. S12. SEM images of CBCNFs following 25 cycles (a, b) and 50 cycles (c, d) under a cycling condition of 1 mA cm^{-2} and 1 mAh cm^{-2}.

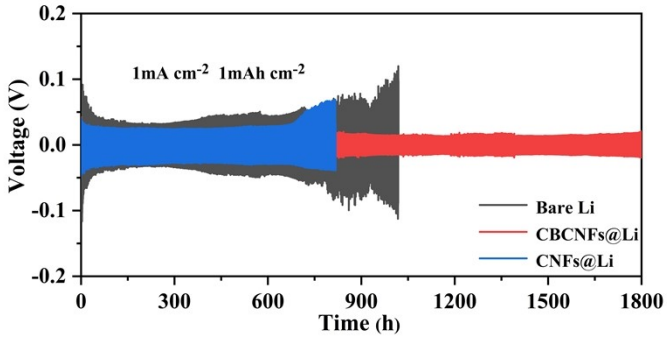

Fig. S13. The deposition/stripping curves of bare lithium, CBCNFs@Li, and CNFs@Li symmetric batteries at a current density of 1 mA cm^{-2} and an area capacity of 1 mAh cm^{-2}.

Table S3 Fitted values of resistances (R_{ct}) using the model in Fig. 6d and Fig. 6e

Material	Fresh R_{ct} (ohm)	25th R_{ct} (ohm)	50th R_{ct} (ohm)	100th R_{ct} (ohm)
Bare Li	115.20	19.52	9.72	6.06
CBCNFs@Li	79.52	13.91	6.93	3.33

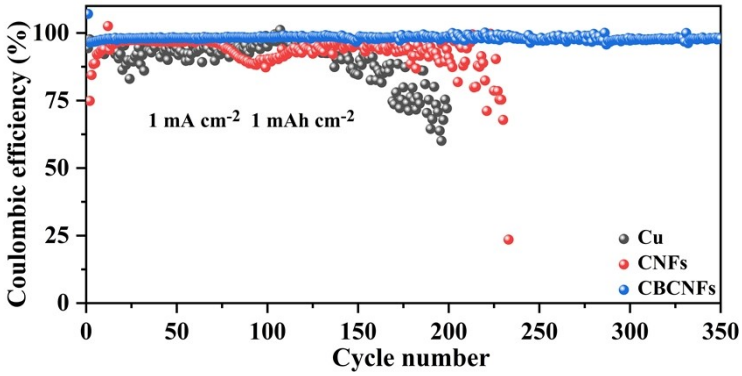

Fig. S14. CE of Cu||Li, CNFs||Li and CBCNFs||Li batteries at current of 1 mA cm^{-2} and capacity of 1 mAh cm^{-2}.

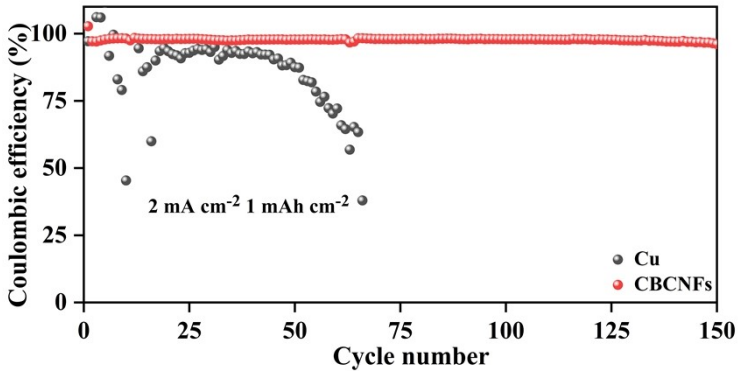

Fig. S15. CE of Cu||Li and CBCNFs||Li batteries at current of 2 mA cm^{-2} and capacity of 1 mAh cm^{-2}.

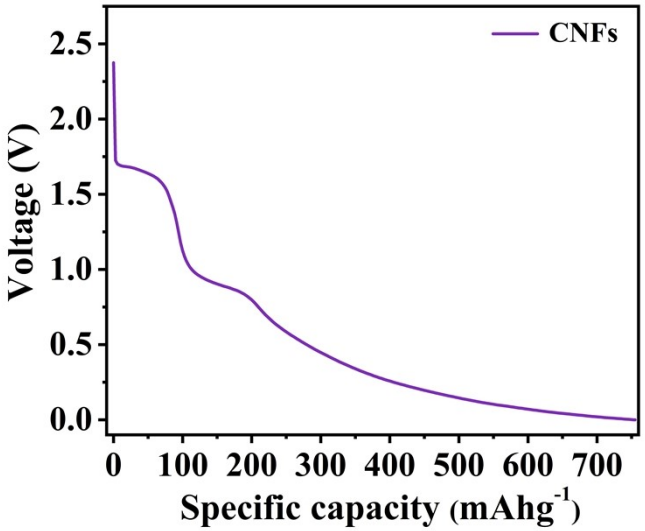

Fig. S16. voltage-specific capacity curve of CNFs||Li cell.

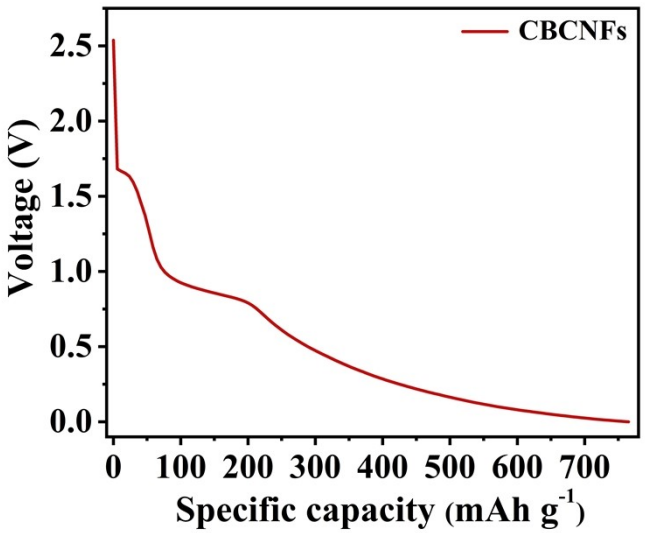

Fig. S17. voltage-specific capacity curve of CBCNFs||Li cell.

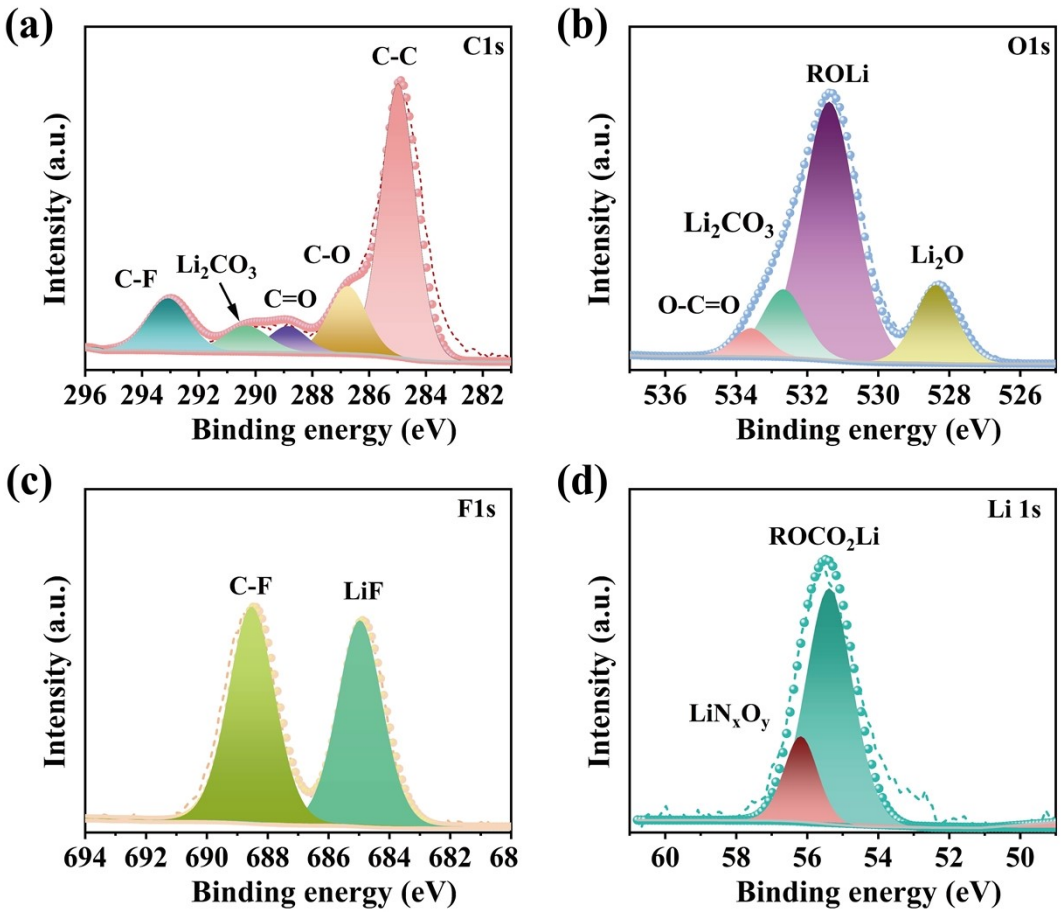

Fig. S18. (a) XPS spectra of the SEI composition on the lithium metal surface after 10 cycles of CBCNFs: (a) C1s spectrum; (b) O1s spectrum; (c) F1s spectrum; (d) Li1s spectrum